

THESIS FOR THE DEGREE OF LICENTIATE OF ENGINEERING

TURBULENT IMPURITY TRANSPORT IN
TOKAMAKS

Albert Mollén



CHALMERS

Department of Applied Physics
Chalmers University of Technology
Göteborg, Sweden, 2013

TURBULENT IMPURITY TRANSPORT IN TOKAMAKS
Albert Mollén

© Albert Mollén, 2013

Technical Report No. CTH-NT-268
ISSN 1653-4662
Nuclear Engineering
Department of Applied Physics
Chalmers University of Technology
SE-412 96 Göteborg
Sweden
Telephone +46-(0)31-772 10 00

Some figures in this thesis are in color only in the electronic version,
available online through Chalmers Publication Library.

Cover:

The image illustrates the impurity distribution in a shot from the
ALCATOR C-Mod tokamak when applying ICRH,
courtesy of M. L. Reinke.
See p. [34](#) for more details.

Printed in Sweden by
Reproservice
Chalmers Tekniska Högskola
Göteborg, Sweden, 2013

Abstract

Nuclear fusion is foreseen as one of the options for future energy production. One of the remaining scientific challenges for establishing the physics basis of future magnetic fusion reactors is to find scenarios where the impurity content in the core can be kept low. High concentration of impurities leads to dilution and radiative energy losses and is detrimental for fusion reactivity. Therefore the understanding and control of impurity transport is of critical importance for the success of fusion.

Impurity transport in fusion plasmas is dominated by turbulent fluctuations. This thesis addresses the effect of poloidal asymmetries and the role of electromagnetic effects on turbulent impurity transport. Transport driven by ion temperature gradient (ITG) mode, trapped electron (TE) mode and kinetic ballooning mode (KBM) turbulence is studied through gyrokinetic modeling. It is shown that poloidal asymmetries significantly affect radial transport, and could be a contributing reason for the experimentally observed decrease of impurity core content in the presence of plasma heating through radiofrequency waves. Furthermore, we show that the value of the ratio of plasma pressure to magnetic pressure can affect the impurity peaking, which is typically found to be lower in KBM turbulence than in ITG turbulence.

Keywords: fusion plasma physics, tokamak, transport, turbulence, gyrokinetic, impurity, poloidal asymmetry

Publications

- [A] A. Mollén, I. Pusztai, T. Fülöp, Ye. O. Kazakov and S. Moradi. Effect of poloidal asymmetries on impurity peaking in tokamaks. *Phys. Plasmas* **19**, 052307 (2012).
http://pop.aip.org/resource/1/phpaen/v19/i5/p052307_s1.
- [B] I. Pusztai, A. Mollén, T. Fülöp and J. Candy. Turbulent transport of impurities and their effect on energy confinement. Accepted for publication in *Plasma Phys. Control. Fusion*, 2013.
<http://arxiv.org/abs/1210.3001>.
- [C] A. Mollén, I. Pusztai, T. Fülöp and S. Moradi. Impurity transport in trapped electron mode driven turbulence. Submitted to *Phys. Plasmas*, 2013.
<http://arxiv.org/abs/1301.1450>.
- [D] S. Moradi, I. Pusztai, A. Mollén and T. Fülöp. Impurity transport due to electromagnetic drift wave turbulence. *Phys. Plasmas* **19**, 032301 (2012).
http://pop.aip.org/resource/1/phpaen/v19/i3/p032301_s1.

Further publications (not included in the thesis)

- [E] S. Moradi, T. Fülöp, A. Mollén and I. Pusztai. A possible mechanism responsible for generating impurity outward flow under radio frequency heating. *Plasma Phys. Control. Fusion* **53**, 115008 (2011).
<http://iopscience.iop.org/0741-3335/53/11/115008>.
- [F] S. Moradi, I. Pusztai, W. Guttenfelder, T. Fülöp and A. Mollén. Micro-tearing modes in spherical and conventional tokamaks. Submitted to *Nucl. Fusion*, 2013.
<http://arxiv.org/abs/1301.1310>.
- [G] T. Fülöp, S. Moradi, A. Mollén and I. Pusztai. The role of poloidal asymmetries in impurity transport. In *Europhysics Conference Abstracts*, volume 35G, page P2.114, Strasbourg, France, 2011.
<http://ocs.ciemat.es/EPS2011PAP/pdf/P2.114.pdf>.
- [H] S. Moradi, T. Fülöp, A. Mollén and I. Pusztai. Possible mechanism responsible for generating impurity outward flow under radio frequency heating. In *14th European Fusion Theory Conference*, Frascati, Italy, 2011.
<http://www.fusione.enea.it/EVENTS/eventifiles/EFTC14-2011/Posters/PRESENTAZIONI%20POSTER/MORADI.pdf>.
- [I] A. Mollén, I. Pusztai, T. Fülöp, Ye. O. Kazakov and S. Moradi. Effect of poloidal asymmetries on impurity peaking in tokamaks. In *Europhysics Conference Abstracts*, volume 36F, page P4.028, Stockholm, Sweden, 2012.
<http://ocs.ciemat.es/EPSICPP2012PAP/pdf/P4.028.pdf>.
- [J] S. Moradi, I. Pusztai, T. Fülöp and A. Mollén. Impurity Transport due to Electromagnetic Drift Wave Turbulence. In *IAEA 24th Fusion Energy Conference*, San Diego, USA, 2012.

Contents

Abstract	iii
Publications	v
Abbreviations	xi
1 Introduction	1
2 Basic theory of magnetized toroidal fusion plasmas	5
2.1 Magnetized fusion plasmas	5
2.2 Charged particle motion in strong magnetic fields	6
2.3 Magnetic geometry	7
2.4 Transport theory	12
2.4.1 Fluid approach	14
2.4.2 Drift kinetic and gyrokinetic approaches	15
2.4.3 Fluxes	15
3 Turbulent transport	17
3.1 Microinstabilities	18
3.1.1 Ion temperature gradient mode	19
3.1.2 Trapped electron mode	20
3.2 Theoretical description	21
3.2.1 Adiabatic response	21
3.2.2 Gyrokinetic description	21
3.3 Ballooning formalism	26
3.3.1 Gyrokinetic equation in ballooning space	27
3.4 Turbulent fluxes	28
3.5 Collisions	30
3.6 Gyrokinetic simulations	32
3.7 Impurity transport	33

4 Summary	37
References	41
Included papers A–D	45

Acknowledgments

My deepest gratitude goes to my supervisors Prof. Tünde Fülöp and Dr. István Pusztai. Tünde is the most dedicated supervisor I can imagine, and it is great to feel her support every day. Besides her deep knowledge she really knows how to tutor students, and I am very happy that she accepted me for joining the Fusion Theory group. István has been an amazing guiding mentor for me in the field of fusion plasma physics. He always seems to have a good answer, whatever weird question one asks.

I would also like to specially thank Dr. Sara Moradi who has been a great help for me during my first years of working with fusion. Furthermore, thanks to Geri, Yevgen, Adam and my other colleagues in the Chalmers Fusion Theory group. It is a pleasure to work with all of you.

Finally I would like to direct some gratitude to the division of Nuclear Engineering at the Applied Physics department. I hope to continue enjoying our common coffee breaks.

Abbreviations

Acronyms

GK	G yro K inetic
ICRH	I on C yclotron R esonance H eating
ITG	I on T emperature G radient
KBM	K inetic B allooning M ode
MHD	M agneto H ydro D ynamic(s)
RF	R adio F requency
TE	T rapped E lectron

Tokamaks

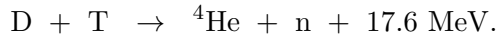
ITER	I nternational T hermonuclear E xperimental R eactor (“The Way” in Latin) Under construction in Cadarache, France
JET	J oint E uropean T orus, Culham Science Centre, Abingdon, UK
JT-60U	Naka, Japan
ALCATOR C-Mod	MIT, Cambridge MA, USA

Chapter 1

Introduction

At present time, mankind is in an increasing demand of energy production. All existing energy sources have their drawbacks, and the search for new sustainable alternatives is one of our most important challenges. Many of today's most utilized technologies put large loads on the environment, and global warming is an evident reality [1].

Thermonuclear fusion is a possible candidate of becoming a long-term option to meet our requirements on energy production. Fusion is the harvest of the high energy content of atomic nuclei, by extracting the energy released when light nuclei combine into heavier ones. In contrast, today existing nuclear reactors implement fission which means splitting heavy nuclei into lighter ones. Fusion has many advantages over fission, specially with respect to safety and radioactive waste, but remains unrealized as a reactor concept even though the idea is about 90 years old [2]. Still the effect of fusion is everyday around us since it is the process which generates the energy of the Sun and the stars. The reason why energy production through fusion on Earth is complicated stems from the high temperatures required to maintain the fusion reactions. The most feasible fusion reaction is between the heavier isotopes of hydrogen, deuterium and tritium [3]:



To overcome the Coulomb repulsion between the positively charged nuclei and sustain the process with a reasonable efficiency, requires a temperature of $\sim 10^8$ K. At this high temperature atoms and molecules are no longer intact, and the medium enters the plasma state of matter consisting of free ions and electrons.

There are three ways to control a fusion plasma: The stars use the gravitational force to confine the plasma, but this method is not practical on Earth. The second method is to compress small fuel pellets to high densities with ultra-intense lasers and utilize the inertia of the matter, it is called inertial confinement. Although a few countries conduct research in this area there is a skepticism about its practicality and cost-effectiveness. The method commonly believed to be the main candidate is instead magnetic confinement.

Magnetic confinement of fusion plasmas take advantage of the fact that the particles of plasmas are charged, and can therefore be controlled by magnetic fields through the Lorentz force. The only three-dimensional topology with non-vanishing continuous tangent vector field is the torus. Accordingly, to prevent high losses, many magnetic confinement devices have toroidal geometries. To date the most successful device is the tokamak with an axisymmetric twisted magnetic field (up to ~ 10 T), created by external coils and an induced plasma current (of the order 10 MA). The twist is necessary in order to avoid losses through particle drifts.

One of the main indicators of how well a fusion device performs is the achieved value of the fusion triple product $n_i T_i \tau_E$, which is the product of the ion density and temperature (i.e. ion pressure) together with the energy confinement time, τ_E . The latter is a measure of how long energy, created from fusion reactions, stays in the plasma and a high enough value is required for the fusion reaction to be self-sustained. The tokamak holding the current world record for highest fusion triple product is the JT-60U experiment in Japan [4]. However, the tokamak with the largest produced fusion power is JET in the UK, which in 1997 produced 16 MW of fusion power – 65% of the input power. JET is also the largest existing fusion experiment. The next step for the magnetic confinement fusion community is ITER under construction in Cadarache, France. It will be an even bigger experiment with the overall goal to demonstrate the technical feasibility of fusion energy production, and is expected to produce 500 MW fusion power from 50 MW input power [5, 6].

To improve confinement, and by that increase the energy confinement time, the radial particle- and energy fluxes should be minimized. The magnetic field lines of a tokamak trace out nested toroidal flux surfaces and a charged particle, if it would not interact with other charged particles, will always be in the close vicinity of a certain flux surface.

However due to the long range nature of the Coulomb force, the charged particles will always interact with each other through Coulomb collisions. The early way of describing transport processes in tokamaks was through a diffusive model based on the Coulomb interaction, the "neo-classical" transport model [7]. From experiments it was soon realized that this model only describes an irreducible minimum to the level of transport experienced in tokamaks, and typically it is overshadowed by a larger level from plasma turbulence. Plasma turbulence can be generated through various kinds of small-scale low-frequency fluctuations, referred to as microinstabilities, which are driven by the density and temperature gradients. Because of the complexity and nonlinearity of plasma turbulence there exist no general theory to describe it, only models with different degree of sophistication. Purely analytical models are too coarse to give a satisfactory explanation and one has to resort to nonlinear kinetic simulation codes. This field has experienced fast progress in recent years, together with the rapid increase of computer performance and development of supercomputers. Nevertheless, reduced models are still important to understand underlying physical mechanisms and ease the interpretation of simulation results.

Besides analyzing the radial fluxes of the main plasma species (i.e. fuel ions and electrons) it is also desirable to describe the behavior of impurity ion species. Impurities are ubiquitous in fusion plasmas, foremost in form of alpha particles (${}^4\text{He}^{2+}$) as a rest product of the D-T fusion reaction, but impurities of higher charge can also enter the plasma by sputtering, arcing and evaporation of the surrounding wall surface, or even artificially by impurity seeding. The presence of impurities leads to plasma dilution and radiative energy losses, and therefore results in a degradation of fusion performance. Specially impurities of high charge are detrimental, mainly because radiation losses are proportional to the square of the charge number, Z^2 [3]. The impurity concentration is typically low compared to the main species, but even a small content can cause severe problems if Z is high. In a steady state, the particle density profiles of a tokamak are usually peaked meaning that the density is highest in the core and decreases in the radial direction. This is also often true for the impurity species. Since the core is the location where most fusion reactions take place (the temperature is also highest in the core) it is undesirable to have impurities accumulating there. In contrast, at the plasma edge impurities can be beneficial through mitigation of the heat loads on the surrounding walls. Consequently it is

interesting to look for scenarios where impurities are transported out of the core into the edge region.

Chapter 2

Basic theory of magnetized toroidal fusion plasmas

The aim of the present chapter is to introduce some fundamental concepts of plasmas, and in particular of toroidally shaped fusion plasmas in strong magnetic fields.

2.1 Magnetized fusion plasmas

A plasma consists of charged particle species, electrons and ions (not necessarily fully ionized), which on a macroscopic level balance each other according to the quasi-neutrality condition [8]

$$n_e = \sum_i Z_i n_i. \quad (2.1)$$

Here n_e is the electron density while n_i and Z_i are the particle density and charge of ion species i (including impurity ions). This condition is valid on length scales significantly larger than the electron Debye length $\lambda_{De} = \sqrt{\epsilon_0 T_e / e^2 n_e}$ and for time scales longer than the inverse plasma frequency $\omega_{pe}^{-1} = \sqrt{m_e \epsilon_0 / e^2 n_e}$, where e is the electron charge, m_e the electron mass and ϵ_0 the vacuum permittivity. For the center of a typical fusion plasma, where the temperature is $T_e \sim 10$ keV and the density $n_e \sim 10^{20} \text{ m}^{-3}$, these quantities can be of the order $\lambda_{De} \sim 10^{-4} \text{ m}$ and $\omega_{pe}^{-1} \sim 10^{-11} \text{ s}$.

Out of all possible nuclear fusion reactions, the one with the largest cross section at reasonably achievable temperatures is between deuterium (D) and tritium (T), the heavier isotopes of hydrogen [3]. Be-

cause of this a future fusion reactor is expected to operate with D-T fuel. However due to the radioactive properties of T and the difficulty of handling it, most fusion plasma experiments today use a single main ion species which is usually either deuterium or ordinary hydrogen. In transport theory it is consequently customary to assume that the main ion species is of charge $Z_i = 1$. Experimentally there will always be an amount of other ions present in the plasma, referred to as impurities, which can enter as a rest product of the fusion reactions or through plasma interaction with the surrounding wall. These impurity species are normally in significantly smaller contents than the main species, but can still have a major impact on the plasma. It is useful to introduce a quantity which is a measure of the purity of the plasma, and this is referred to as the effective ion charge $Z_{\text{eff}} = \sum_i Z_i^2 n_i / n_e$. For a pure hydrogenic plasma $Z_{\text{eff}} = 1$, and it increases with the impurity content. The Bremsstrahlung radiation losses are directly proportional to Z_{eff} , and because of this the presence of high- Z impurities can lead to severe energy losses through radiation, even in small quantities. Moreover impurities also dilute the plasma, and together these effects can result in a heavy degradation of fusion reactivity.

2.2 Charged particle motion in strong magnetic fields

The motion of charged particles in a strong magnetic field is characterized by rapid gyration around the magnetic field lines. In a homogeneous magnetic field of strength B , the gyration frequency of species α is given by $\Omega_\alpha = e_\alpha B / m_\alpha$, and is consequently a function of charge and mass [7]. The Larmor radius of the gyration is $\rho_\alpha = v_\perp / \Omega_\alpha$, where v_\perp denotes the magnitude of the particle velocity component perpendicular to the magnetic field. In a strongly magnetized plasma the Coulomb collision frequency of species α should be much smaller than the gyro-frequency, $\nu_\alpha \ll \Omega_\alpha$, and the ion Larmor radius ($\rho_e \ll \rho_i$) should be much smaller than the characteristic length scale on which equilibrium plasma parameters vary (e.g. density scale length $L_{n\alpha} = |\nabla \ln n_\alpha|^{-1}$ and temperature scale length $L_{T\alpha} = |\nabla \ln T_\alpha|^{-1}$), $\rho_i \ll L$. We will show later that these assumptions permit doing expansions in the smallness of certain parameters, useful in transport theory.

It is convenient to decompose the particle position into the *guiding*

center position and the *gyro* motion, $\mathbf{r} = \mathbf{R} + \mathbf{b} \times \mathbf{v} / \Omega_\alpha \equiv \mathbf{R} + \boldsymbol{\rho}$ with $\mathbf{b} = \mathbf{B}/B$. In a homogeneous magnetic field the guiding center motion will be simply given by $\dot{\mathbf{R}} = v_\parallel \mathbf{b}$, where v_\parallel is the magnitude of the particle velocity component parallel to the magnetic field. In spatially varying magnetic fields and in the presence of electric fields, perpendicular drifts and the magnetic mirror force arise. The perpendicular drift velocity can be written

$$\mathbf{v}_d = \dot{\mathbf{R}}_\perp = \frac{\mathbf{E} \times \mathbf{B}}{B^2} + \frac{v_\perp^2}{2\Omega_\alpha} \mathbf{b} \times \nabla \ln B + \frac{v_\parallel^2}{\Omega_\alpha} \mathbf{b} \times \boldsymbol{\kappa}, \quad (2.2)$$

where the derivation assumes that the drift velocity is small compared to the particle velocity, $|\mathbf{v}_d| \ll |\mathbf{v}|$. Here $\boldsymbol{\kappa} = -\mathbf{b} \times (\nabla \times \mathbf{b})$ is the curvature vector of the magnetic field. The first term in Eq. 2.2 is the $\mathbf{E} \times \mathbf{B}$ drift velocity, independent of the particle charge and mass. The other two terms together represent the magnetic drift velocity due to inhomogeneities in the magnetic field, composed of the grad- B drift and the curvature drift. Because of their $1/\Omega_\alpha$ dependence they depend on the particle charge and mass, and are in opposite direction for electrons and ions.

The magnetic mirror force acts in the direction parallel to the magnetic field and its magnitude is $\mu \nabla_\parallel B$, where $\mu = m_\alpha v_\perp^2 / (2B)$ is the magnetic moment of the gyrating particle. The force arises because the magnetic moment is an adiabatic invariant, meaning that over slow spatial and temporal changes of magnetic field strength the particle velocity will change to keep μ constant. This combined with the preservation of the total particle energy $\mathcal{E} = m_\alpha v^2 / 2 + e_\alpha \phi$, with ϕ being the electrostatic potential, results in a counteraction of particle motion with the gradient of B .

2.3 Magnetic geometry

The magnetic fields of a toroidal axisymmetric magnetic fusion device closely describe an ideal toroidal magnetohydrodynamic (MHD) equilibrium [9], where the plasma particle pressure p is balanced by a magnetic force according to

$$\mathbf{j} \times \mathbf{B} = \nabla p, \quad (2.3)$$

where \mathbf{j} is the total current density. It is possible to show that as a consequence, the magnetic geometry of an axisymmetric magnetic fusion device is characterized by closed field lines that lie within a doughnut

shape, where the long way around is referred to as the toroidal direction and the short way as the poloidal direction. It is useful to introduce toroidal/poloidal coordinates (r, θ, φ) which relates to Cartesian coordinates (x, y, z) by

$$\begin{aligned}x &= (R_0 + r \cos \theta) \cos \varphi \\y &= (R_0 + r \cos \theta) \sin \varphi \\z &= r \sin \theta.\end{aligned}\tag{2.4}$$

The physical quantities are 2π -periodic in the toroidal angle φ and poloidal angle θ for fixed r . R_0 and r denote the major and minor radii, and $r = a$ at the edge of a device with circular cross section (which is usually not valid in real experiments but often used as an approximation in theory). The parameters are illustrated in Fig. 2.1. The ratio R_0/r is normally referred to as the aspect ratio while $\epsilon = r/R_0$ is the inverse aspect ratio, in theory it is common to analyze the large-aspect-ratio limit ($\epsilon \ll 1$). A tokamak has a twisted magnetic field, i.e. both a toroidal B_φ and a poloidal B_θ component, in order to cancel out the particle drifts described by Eq. 2.2 on a particle orbit average. A purely toroidal field would result in charge separation through the magnetic drifts and a rising electric field, this field then leads to severe radial losses by the $\mathbf{E} \times \mathbf{B}$ drift. Because of the twist, particles spend half of their time drifting away from a given radial location, and half of their time approaching it. The field lines trace out magnetic surfaces referred to as *flux surfaces* (this concept is illustrated in Fig. 2.1). These are surfaces of constant particle pressure which the currents flow within. Even the density and temperature of each species are in the usual situation approximately constant over a flux surface. However, as will be further discussed in this thesis, there are physical phenomena (e.g. plasma rotation and RF heating) that can cause significant asymmetries to arise for certain species. Specially high- Z impurities are prone to be affected, due to their large charge and mass.

Experimentally the flux surfaces are normally not circular over a cross section and it is customary to use a flux function as radial coordinate (instead of r in Eq. 2.4), which is constant on a flux surface. The common choice is the poloidal magnetic flux between the surface and the magnetic axis divided by 2π , $\psi = \Psi_p/2\pi$, but another convenient choice is the toroidal flux $\chi_t = \Psi_T/2\pi$. Considering an infinitesimal annulus between two flux surfaces separated by dr , as illustrated in Fig. 2.2, the differential poloidal flux is written $d\Psi_p = 2\pi R B_\theta dr$ [8]. Both ψ and χ_t are radially monotonously increasing and can be written as functions

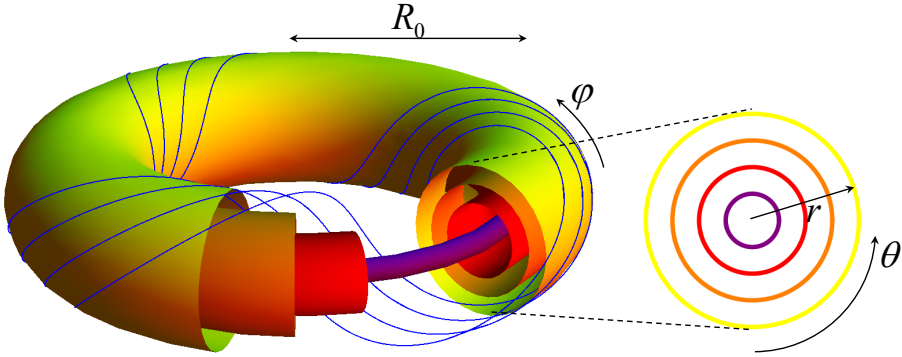


Figure 2.1: Toroidal geometry, with the parameters (r, θ, φ) , illustrating twisted magnetic field lines and the concept of flux surfaces. Observe that the twist has been exaggerated and in reality there is typically less than one poloidal turn per toroidal turn.

of each other. It can be shown that a possible vector potential associated with \mathbf{B} , i.e. $\mathbf{B} = \nabla \times \mathbf{A}$, is $\mathbf{A} = \chi_t \nabla \theta - \psi \nabla \varphi$ [9]. An important flux surface parameter is the *safety factor*, $q(\psi) = d\chi_t(\psi)/d\psi$, which is a measure of the helical "twistedness" of the field lines. The safety factor is dimensionless and tells how many toroidal turns are required to encircle the flux surface once poloidally, when following a magnetic field line. In the large-aspect-ratio limit the safety factor can be approximated as $q \approx (rB_\varphi)/(R_0B_\theta)$. To avoid major instabilities the safety factor should be kept above 1 everywhere in a tokamak, this means that the toroidal magnetic field component has to be significantly larger than the poloidal component. Another important parameter is the magnetic shear, $s = r d(\ln q)/dr$, saying how q changes radially when changing flux surface. In tokamaks s is usually positive implying that q increases monotonously from the center to the edge, however there are scenarios where a negative s can be beneficial.

A common geometry to analyze theoretically (which we employ in this thesis) is the large-aspect-ratio limit with circular cross section and small plasma pressure compared to the magnetic field pressure ($\beta \equiv 2\mu_0 p/B^2 \ll 1$). Then the equilibrium is very simple and the magnetic field strength is given by $B = B_0/(1 + \epsilon \cos \theta)$, with B_0 being the field strength on the axis. Most tokamaks however are non-circular and β can be a few percent. For shaped equilibria and high β one must solve the *Grad-Shafranov equation* [8] to find the equilibrium, codes simulating tokamak transport usually have a model to parameterize the plasma in

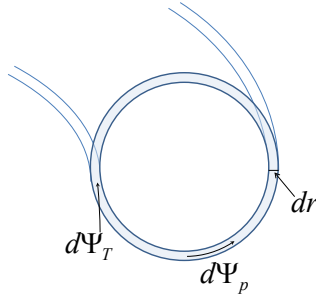


Figure 2.2: Flux annulus of width dr containing the poloidal flux $d\Psi_p$ and toroidal flux $d\Psi_T$ (adapted from [8]).

this equilibrium.

The magnetic field strength is inversely proportional to $R = \sqrt{x^2 + y^2}$, i.e. $B \propto 1/R$. As a consequence of this, the mirror force described earlier gives rise to the phenomenon of *trapped particles*. The trapped particles are particles with so high magnetic moment as compared to their kinetic energy, that they are not able to make a complete poloidal turn before they are reflected back by the mirror force. They are therefore trapped on the low-field-side, which implies that they bounce back and forth in the outboard side of the torus. The poloidal projections of their guiding center trajectories have banana shapes and are commonly referred to as *banana orbits* [7]. The phenomenon is illustrated in Fig. 2.3. The trapped particles constitute a fraction $\sim \sqrt{\epsilon}$ of the total number of particles which is normally small, still they can be responsible for a major part of the radial transport.

The drifts described by Eq. 2.2 apply to single charged particles in a strong magnetic field. Often it is useful to describe a fusion plasma through a statistical approach or as a fluid, rather than a collection of discrete particles. It is then possible to see that another macroscopic drift arises, which is present even in the absence of single particle guiding center drifts. This drift is called the *diamagnetic drift* and is due to the inevitable pressure gradient (i.e. gradient of density and/or temperature) present in magnetic fusion plasmas. The name of the drift stems from the fact that plasmas are naturally diamagnetic, i.e. the gyro orbits of the charged particles produce small magnetic fields being in the opposite direction to the total magnetic field [8]. The drift can be understood from the simple picture in Fig. 2.4 [1]. If the plasma density is larger at the top than at the bottom, there are more ions going to the left than to

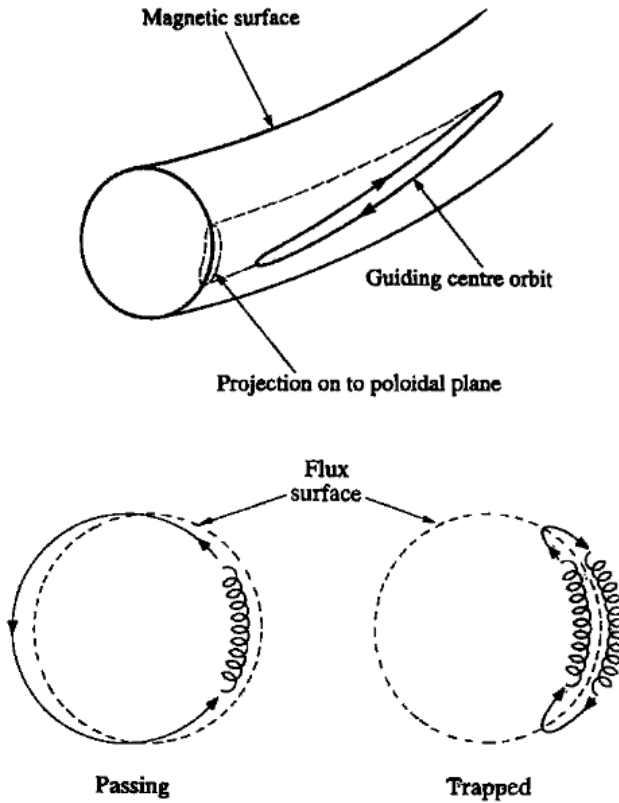


Figure 2.3: The upper figure shows the banana orbit of a trapped particle, illustrating how it bounces back and forth on the low-field-side of the torus. The lower figure shows the poloidal projection for the orbit of a passing particle (left) and trapped particle (right) (figures from [8]).

the right. Similarly if the plasma temperature is larger at the top, the ions going to the left have larger velocity on average than the ions going to the right. The ion fluid in a small volume element consequently has an average flow towards left. This is the ion diamagnetic drift, denoted by v_{Di} . The electron diamagnetic drift v_{De} is in the opposite direction, due to the negative charge and the corresponding reversed direction of the electron gyration.

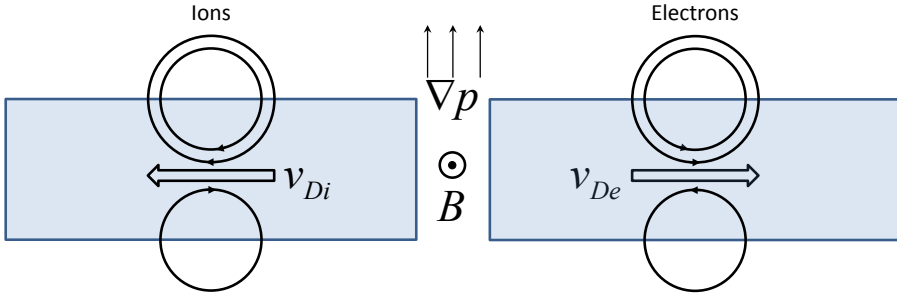


Figure 2.4: Illustration of how the diamagnetic drift arise (adapted from [1]). Note that the electron gyro orbit has been exaggerated, as compared to the ion.

2.4 Transport theory

A major part of the theoretical work for toroidal magnetized fusion plasmas is directed towards the understanding of the radial transport of particles and energy. It is intuitive to realize that to maximize the energy confinement time, one should search for configurations where the outward radial transport of electrons and main ions is minimized. At the same time it is desirable with transport of impurities out of the core to the edge of a plasma. The largest contribution to the radial transport is usually caused by small scale collective instabilities, typically driven by the gradients of density and temperature. A main objective of transport theory is to understand and predict the numerous different instabilities that can arise in a fusion plasma. Large scale magnetohydrodynamic (MHD) instabilities can also occur, sometimes leading to disruptions which can cause termination of a tokamak plasma and should consequently be avoided. These instabilities can be prevented by operating the plasma in the right regimes.

Since a fusion plasma is a collection of $\sim 10^{20}$ charged particles it

is not possible to follow the evolution of each individual particle in a tractable way. The most sophisticated existing description is the kinetic theory which describes each plasma species α through its phase space distribution function $f_\alpha(t, \mathbf{r}, \mathbf{v})$, where t is time, \mathbf{r} position and \mathbf{v} velocity. From the distribution function macroscopic quantities, such as densities, fluxes, flows and currents, can be determined by taking appropriate moments and averages. The evolution of the distribution function is determined from the *Fokker-Planck equation* [8]

$$\frac{df_\alpha}{dt} \equiv \frac{\partial f_\alpha}{\partial t} + \mathbf{v} \cdot \nabla f_\alpha + \frac{e_\alpha}{m_\alpha} (\mathbf{E} + \mathbf{v} \times \mathbf{B}) \cdot \frac{\partial f_\alpha}{\partial \mathbf{v}} = C_\alpha[f_\alpha], \quad (2.5)$$

where e_α and m_α are the charge and mass of the species, and $e_\alpha(\mathbf{E} + \mathbf{v} \times \mathbf{B})/m_\alpha$ is the acceleration due to the Lorentz force. $C_\alpha[f_\alpha] = \sum_b C_{\alpha b}[f_\alpha, f_b]$ is the *Coulomb collision operator* describing the change in distribution as a result of Coulomb collisions with all plasma species ($C_{\alpha b}[f_\alpha, f_b]$ describes collisions of species α on species b). \mathbf{E} and \mathbf{B} represent the macroscopic electric and magnetic fields. The microscopic parts of these fields, which are fluctuating on spatial scales comparable to or smaller than the Debye length, are contained in the collision operator. A plasma is completely described in a self-consistent way by the Fokker-Planck equation coupled with Maxwell's equations. The problem is that this system of equations is highly complex and tedious to treat in reality, and often one resorts to different simplifications.

In collisional transport theory, appropriate for quiescent plasmas, the macroscopic fields in Eq. 2.5 are often not determined self-consistently by coupling to Maxwell's equations [10]. In *classical* theory the fields are simply replaced by given external fields, $\mathbf{E} \approx \mathbf{E}_0$ and $\mathbf{B} \approx \mathbf{B}_0$, where $\mathbf{E}_0, \mathbf{B}_0$ are stationary and homogeneous. *Neoclassical* transport theory takes the toroidal magnetic geometry into account, with \mathbf{E} and \mathbf{B} obtained from an equilibrium solution of the macroscopic MHD equations. Common to these approaches is that the fields are determined independently of the particle distribution functions, and then substituted into Eq. 2.5 as given functions.

In contrast to collisional transport theory, turbulent transport theory (discussed in Chapter 3) introduces fluctuating fields into Eq. 2.5 and couples it to Maxwell's equations. For a turbulent plasma a statistical description is best suited.

2.4.1 Fluid approach

As earlier mentioned we obtain interesting macroscopic quantities by taking velocity moments of f_α , i.e. integrating over velocity space: $\int d^3v \equiv \int_{-\infty}^{\infty} dv_{\parallel} \int_0^{\infty} dv_{\perp} v_{\perp} \int_0^{2\pi} d\zeta$. For example, the particle density is obtained as the 0th moment, $n_\alpha(t, \mathbf{r}) = \int f_\alpha(t, \mathbf{r}, \mathbf{v}) d^3v$. It is convenient to denote the average of a quantity A over the particle distribution by $\langle A \rangle_f \equiv \int A f_\alpha d^3v / n_\alpha$. Now the local particle temperature can be defined as $T_\alpha(t, \mathbf{r}) \equiv \langle m_\alpha (\mathbf{v} - \mathbf{V}_\alpha)^2 \rangle_f / 3$, where $\mathbf{V}_\alpha(t, \mathbf{r}) = \langle \mathbf{v} \rangle_f$ is the macroscopic fluid velocity.

One way to proceed from Eq. 2.5 is by forming velocity moments of the equation, and by this approach we obtain fluid equations. The $\{1, m\mathbf{v}, mv^2/2\}$ velocity moments of Eq. 2.5 describe the conservation properties of particles, momentum and energy [7]

$$\frac{\partial n_\alpha}{\partial t} + \nabla \cdot (n_\alpha \mathbf{V}_\alpha) = 0, \quad (2.6)$$

$$\frac{\partial m_\alpha n_\alpha \mathbf{V}_\alpha}{\partial t} + \nabla \cdot \mathbf{\Pi}_\alpha = n_\alpha e_\alpha (\mathbf{E} + \mathbf{V}_\alpha \times \mathbf{B}) + \int d^3v C_\alpha [f_\alpha] m_\alpha \mathbf{v}, \quad (2.7)$$

$$\frac{\partial}{\partial t} \left(\frac{3n_\alpha T_\alpha}{2} + \frac{m_\alpha n_\alpha V_\alpha^2}{2} \right) + \nabla \cdot \mathbf{Q}_\alpha = n_\alpha e_\alpha \mathbf{E} \cdot \mathbf{V}_\alpha + \int d^3v C_\alpha [f_\alpha] \frac{m_\alpha v^2}{2}. \quad (2.8)$$

Here we have introduced the momentum flux tensor $(\mathbf{\Pi}_\alpha)_{jk} \equiv \langle m_\alpha n_\alpha v_j v_k \rangle_f$ and the energy flux $\mathbf{Q}_\alpha \equiv m_\alpha n_\alpha \langle v^2 \mathbf{v} \rangle_f / 2$. The last terms of Eq. 2.7 and Eq. 2.8 can be rewritten by introducing the friction force $\mathbf{R}_\alpha \equiv \int d^3v C_\alpha [f_\alpha] m_\alpha \mathbf{v}$ and the rate of thermal energy transfer $\mathcal{Q}_\alpha \equiv \int d^3v C_\alpha [f_\alpha] m_\alpha |\mathbf{v} - \mathbf{V}_\alpha|^2 / 2 = \int d^3v C_\alpha [f_\alpha] m_\alpha v^2 / 2 - \mathbf{R}_\alpha \cdot \mathbf{V}_\alpha$, consequently these quantities describe the Coulomb interaction with other species.

One important objective of transport theory is to determine the space-time evolution of n_α , \mathbf{V}_α and T_α for all plasma species. To perform simulations based on the fluid equations is a widespread approach, but the major issue with the fluid equations is that each moment equation couples to one higher up in the hierarchy. This means that it is not possible to obtain a closed system of equations, since we would need to

take an infinite number of moments. To obtain closure one must introduce approximations. That is the reason why a kinetic approach is more sophisticated, but at the same time more expensive to use.

2.4.2 Drift kinetic and gyrokinetic approaches

To describe transport processes in fusion plasmas, it is usually not necessary to resolve time scales comparable to or faster than the rapid ion gyro motion. By making use of the smallness of the Larmor radius as compared to the typical length scales, a gyro-phase averaging can be performed on the kinetic equation. This implies that we only follow the distribution of particle guiding centers and ignore the gyro-phase, thus reducing the description from 6D phase-space to 5 dimensions. In collisional transport theory considering toroidally symmetric fields the so called drift kinetic equation is mainly used, representing particles as drifting guiding centers with a charge and magnetic dipole moment. For turbulent transport, which we will treat in Chapter 3, the gyrokinetic equation is more suitable because it allows for sharp spatial variations in perturbed fields and also for distributions on as small scale as the electron Larmor radius.

2.4.3 Fluxes

The different fluxes in a plasma are produced by the thermodynamic forces, related to the spatial inhomogeneities such as the density and temperature gradients, ∇n_α and ∇T_α . As examples, from a simple random walk estimate we can derive Fick's law [7, 10] relating the local diffusive collisional particle flux with the density gradient

$$\Gamma_\alpha = -D_\alpha \nabla n_\alpha, \quad (2.9)$$

and Fourier's law relating the local heat flux with the temperature gradient

$$\mathbf{q}_\alpha = -n_\alpha \chi_\alpha \nabla T_\alpha. \quad (2.10)$$

Here D_α is called the diffusion coefficient and χ_α the heat diffusivity.

We now let $\langle A \rangle$ denote the flux surface average of a quantity A . The most important transport quantities of a magnetic fusion plasma are the flux surface average of the cross-field particle and energy fluxes which we denote by $\Gamma_{\alpha\perp}$ and $Q_{\alpha\perp}$ respectively. If we know the species distribution

function they can readily be calculated as

$$\Gamma_{\alpha\perp} \equiv \langle \Gamma_\alpha \cdot \nabla\psi \rangle = \left\langle \int d^3v f_\alpha \mathbf{v} \cdot \nabla\psi \right\rangle \quad (2.11)$$

and

$$Q_{\alpha\perp} \equiv \langle Q_\alpha \cdot \nabla\psi \rangle = \left\langle \int d^3v \frac{m_\alpha v^2}{2} f_\alpha \mathbf{v} \cdot \nabla\psi \right\rangle. \quad (2.12)$$

It is often the case that the cross-field particle flux can be divided into separate contributions as,

$$\Gamma_{\alpha\perp} = -D_\alpha \nabla_\perp n_\alpha - H_\alpha \nabla_\perp T_\alpha - n_\alpha V_\alpha. \quad (2.13)$$

The three terms on the right hand side of Eq. 2.13 represent diffusion, thermodiffusion and convective flux (“pinch flux”) respectively. The coefficients D_α , H_α and V_α are free to depend on other plasma parameters.

Chapter 3

Turbulent transport

Experimentally measured radial fluxes of particles and energy are usually greater than what would be expected from collisional transport theory [9]. This enhanced anomalous transport is attributed to small-scale turbulent fluctuations called microinstabilities. These instabilities saturate at a low amplitude, as compared to background average quantities, due to nonlinear mechanisms. The fluctuating electric fields make the particles $\mathbf{E} \times \mathbf{B}$ drift radially in a random manner. The fluctuation amplitude is typically small, with $\delta n/n_0$ (ratio of fluctuating and mean parts of the density) being less than 1% in the core. Closer to the edge the amplitude of the fluctuations can be larger, but in this thesis the main focus is on core turbulence. In the absence of turbulent fluctuations neoclassical transport dominates.

The number of different kinds of *modes* (or waves) that can exist in a plasma is large, as compared to vacuum where only electromagnetic waves can propagate [10]. In a Fourier description each mode is characterized by its wave vector \mathbf{k} and frequency $\omega = \omega_r + i\gamma$, and the *dispersion equation* relating them. Any plasmadynamical quantity Q (e.g. density, pressure, velocity, electric potential,...) can be represented in the form $Q = Q_0 + \delta Q$, where $Q_0 = \langle Q \rangle_{ens}$ is the ensemble average of Q and δQ is a deviation from Q_0 (the fluctuation). In a linear description, where the perturbations remain small, $\delta Q \propto \exp(i\mathbf{k} \cdot \mathbf{r} - i\omega t)$. Then ω_r is the fluctuation frequency while γ is either the damping rate, if $\gamma < 0$, or growth rate, if $\gamma > 0$. The latter case characterizes an unstable mode. For a linearly unstable mode, the amplitude of δQ will grow in time, and therefore the nonlinear terms (previously neglected) will become more important and lead to interactions between several linear modes. This

generally leads to a complex rearrangement of the plasma structure and the state becomes truly turbulent. The level of transport is determined by the saturation amplitude of the perturbed quantities and assuming different saturation mechanisms result in different diffusivities.

3.1 Microinstabilities

In a spatially inhomogeneous plasma, so called *drift waves* appear. They are driven by the free energy source stored in the gradients, and play a crucial role in the mechanism of anomalous transport. The free energy can become accessible for waves, which can then be destabilized. This can be provided through mechanisms such as unfavorable magnetic curvature and parallel compressibility. We can classify microinstabilities into various modes according to the variety of free energy source, accessibility mechanism and magnetic geometry. Two of the most important electrostatic drift wave types are the ion temperature gradient (ITG) mode and the trapped electron (TE) mode, and they will be further discussed in this thesis.

The microinstabilities have spatial scales which are typically significantly longer than the Debye length and are relatively slow, so that quasineutrality $\sum_{\alpha} e_{\alpha} \delta n_{\alpha} = 0$ (where δn_{α} is the perturbed density) is a good approximation. Quasineutrality can therefore be used to obtain an electrostatic dispersion relation from the density responses of the different species. Furthermore the microinstabilities have much lower frequencies than the gyro frequencies (Ω_e, Ω_i), and it is therefore appropriate to use gyro-averaged equations. Several types of microinstabilities also have lower frequency than the trapped electron bounce frequency, allowing for bounce averaged electron equations. As a consequence of this averaging operator the parallel dynamics is annihilated for trapped electrons.

When analyzing microinstabilities it is sometimes sufficient to focus on electrostatic perturbations and neglect magnetic field perturbations. In Appendix A of Ref. [10] an order-of-magnitude estimate is presented which shows that $(|\delta \mathbf{B}|/B)/(\delta n_e/n) \sim \beta$, and since β is usually small we conclude that the electrostatic approximation is often valid. Still there are scenarios when β can be relatively high and simulation codes often allow for the inclusion of magnetic field perturbations. In the present thesis the main focus is on electrostatic turbulence and this is what will be mostly discussed, but paper D includes a study of electro-

magnetic turbulence.

3.1.1 Ion temperature gradient mode

As the name suggests the ITG mode is driven by the ion temperature gradient. High central ion temperature is a requirement for magnetic fusion and therefore large temperature gradients will be present. The ITG modes are of primary interest and believed to be the major contributor to anomalous ion thermal transport. ITG modes are sometimes called η_i modes, where $\eta_i \equiv d \ln T_i / d \ln n_i$, because they only occur if η_i exceeds a certain value of order unity. The ITG modes primarily arise due to bad magnetic curvature, destabilized by ∇B and curvature drifts, or by parallel ion dynamics resonance. In the former case it is called toroidal ITG mode since it is related to the geometry, while the latter case is called slab ITG and appears even if the magnetic curvature is neglected.

The toroidal ITG mode can be interpreted as follows. The bad magnetic curvature of a tokamak is on the outboard, low-field side of the torus. If a temperature perturbation emerge there, the magnetic drift of particles have different velocities in different temperature regions. This leads to a growing density perturbation out of phase with the temperature perturbation. As a consequence of the density perturbation, a potential perturbation is generated leading to $\mathbf{E} \times \mathbf{B}$ drift flows. The phase between the perturbed flows and the temperature perturbation is such that hot plasma transports to already higher temperature spots of the perturbation. This results in a feedback mechanism leading to a growing perturbation amplitude, and thus an instability. On the inboard side of the torus, the direction of ∇T is opposite to that of ∇B , and the feedback mechanism disappear. The dependence of the ITG drive on poloidal angle is one of the reasons why it typically has the "ballooning" form of the mode structure.

A toroidal ITG mode typically has a frequency of $\omega \sim k_\theta \rho_i v_{Ti} / R$, where k_θ is the poloidal mode number and v_{Ti} the thermal ion velocity. It propagates in the ion diamagnetic direction. When the mode frequency falls below the trapped ion bounce frequency, $\omega_{bi} = v_{Ti} \sqrt{\epsilon} / (qR)$, trapped ion effects become destabilizing and the mode gradually evolves into a trapped ion mode (TIM).

3.1.2 Trapped electron mode

When the mode frequency is comparable to or lower than the trapped particle bounce frequency, trapping effects become important. Trapped particles spend most of their time in the bad curvature region on the low field side of a torus, thus the magnetic curvature drift is not averaged out as for passing particles. Local electric fields arise leading to $\mathbf{E} \times \mathbf{B}$ drifts and resulting in microinstabilities.

The trapped electron response is the dominant contribution to the non-adiabatic electron response [11]. Therefore the TE mode, primarily driven by the trapped electron toroidal precession resonance, is of interest. The TE modes appear in the same wave number range as the ITG modes, $k_{\theta}\rho_i \lesssim 1$, and with a similar frequency. TE modes can be the dominant instabilities in scenarios where η_i is small, so that ITG modes do not occur, and if the effective electron collisionality ν_{eff} is low enough. Too frequent collisions lead to de-trapping of the trapped electrons under a bounce period and thus to removal of the trapped electron drive. The TE modes are typically driven by the density gradients $1/L_n$ and/or the electron temperature gradient $1/L_{Te}$. Unlike ITG modes, TE modes propagate in the electron diamagnetic direction.

TE modes can be divided into the dissipative (DTEM) and collisionless (CTEM) classes. In the former energy is transferred from trapped electrons to waves via trapped electron collisions, and it requires a strong electron temperature gradient and high collisionality. Still the collisionality has to be low enough for the trapped electrons to execute a bounce period before getting de-trapped. On average the typical trapped electrons get de-trapped by collisions during one wave period but not during the shorter bounce motion period. For the latter class energy is transferred to waves through wave-precession-drift resonance, and this type is more likely to be destabilized in reactor relevant conditions with low collisionality. Here collisions must be rare enough for trapped electrons to precession drift around the torus more than once before getting de-trapped by collisions. The collisionless TE mode is investigated carefully in paper C and shown to be stabilized by increasing collisionality.

3.2 Theoretical description

3.2.1 Adiabatic response

Since electrons can adjust quickly to potential variations, due to their high velocity, a common approximation to make is the Boltzmann response for the electron density

$$\frac{\delta n_e}{n_0} = \frac{|e| \delta \phi}{T_e}, \quad (3.1)$$

where $\delta \phi$ is the fluctuating electrostatic potential (note that in the papers we refer to this simply as ϕ). This is called the adiabatic response because of the reference to the relative slow timescale of a drift wave compared to the electron transit motion, $\omega \ll k_{\parallel} v_{Te}$ where v_{Te} is the thermal electron velocity and k_{\parallel} the parallel wave number. Note that, unlike electron drift waves, ITG modes can be driven unstable even with adiabatic electron response.

A typical consequence of the adiabatic assumption is, as we will see later, that it does not lead to any cross-field transport.

3.2.2 Gyrokinetic description

The gyrokinetic framework is particularly suitable to describe turbulent fluctuations in plasmas, and the approach is based on the assumption that the equilibrium quantities are slowly varying, while the perturbations are smaller but more rapidly varying in space. The idea of gyrokinetics is that on the time scales and length scales of interest (here for the turbulent fluctuations), it is typically not necessary to follow the rapid gyro motion of particles, but rather look at the distribution of the guiding centers. The equations can therefore be averaged over the gyro-phase, thus reducing the description from 6D phase-space to 5D. The equations can advantageously be derived using a different coordinate system, such as guiding center coordinates $(\mathbf{R}, \mathcal{E}, \mu, \zeta)$ (where ζ is the gyro-phase, i.e. $\mathbf{v} = v_{\parallel} \mathbf{b} + v_{\perp} [\mathbf{e}_1 \cos \zeta + \mathbf{e}_2 \sin \zeta]$), and in different magnetic geometries. Here we are naturally most interested in the toroidal geometry. These equations can be derived using a recursive technique. The equations presented in the present section are based on [12, 13].

As earlier mentioned, the fluctuating fields can be decomposed into an ensemble average and a fluctuation

$$\begin{aligned} \mathbf{E} &= \mathbf{E}_0 + \delta \mathbf{E}, & \phi &= \phi_0 + \delta \phi, \\ \mathbf{B} &= \mathbf{B}_0 + \delta \mathbf{B}, & \mathbf{A} &= \mathbf{A}_0 + \delta \mathbf{A}, \end{aligned} \quad (3.2)$$

with $\mathbf{E} = -\nabla\phi - \partial\mathbf{A}/\partial t$ and $\mathbf{B} = \nabla \times \mathbf{A}$ (in the electrostatic approximation $\delta\mathbf{B} = \delta\mathbf{A} = 0$). Similarly the distribution function of species α is decomposed into

$$f_\alpha = F_\alpha + \delta f_\alpha, \quad (3.3)$$

where F_α is the ensemble-average of f_α .

To describe the ordering of gyrokinetic theory it is convenient to introduce the ion sound speed $c_s = \sqrt{T_e/m_i}$ and the ion sound Larmor radius $\rho_s = c_s/\Omega_i \sim \rho_i\sqrt{T_e/T_i}$. The derivation of the gyrokinetic equation is based on an expansion of the Fokker-Planck equation in the smallness of $\rho_* = \rho_s/a$ (remember that a is the plasma minor radius, and thus signifies a typical length scale of the system). The ordering of gyrokinetic theory is written as

$$\frac{\delta f_\alpha}{F_\alpha} \sim \frac{e_\alpha \delta\phi}{T_\alpha} \sim \frac{e_\alpha v_{T\alpha} |\delta\mathbf{A}|}{T_\alpha} \sim \frac{k_{\parallel}}{k_{\perp}} \sim \frac{\omega}{\Omega_\alpha} \sim \rho_*, \quad (3.4)$$

when the ensemble-averaged quantities change only due to fluxes driven by fluctuations of sizes described by Eq. 3.4, they must vary slowly as $\partial/\partial t \sim \rho_*^2$.

The Fokker-Planck equation (Eq. 2.5) is written as

$$\left\{ \frac{\partial}{\partial t} + \mathbf{v} \cdot \nabla + \frac{e_\alpha}{m_\alpha} [(\mathbf{E}_0 + \delta\mathbf{E}) + \mathbf{v} \times (\mathbf{B}_0 + \delta\mathbf{B})] \cdot \frac{\partial}{\partial \mathbf{v}} \right\} (F_\alpha + \delta f_\alpha) = C_\alpha [F_\alpha + \delta f_\alpha]. \quad (3.5)$$

The general approach is to separate Eq. 3.5 into two components, the ensemble-average (equilibrium) part, \mathcal{A} , and the fluctuating (perturbed) part, \mathcal{F} ,

$$\mathcal{A} = \frac{d}{dt} \Big|_{ens} F_\alpha - \langle C_\alpha \rangle_{ens} - \mathcal{D}_\alpha, \quad (3.6)$$

$$\mathcal{F} = \frac{d}{dt} \Big|_{ens} \delta f_\alpha + \frac{e_\alpha}{m_\alpha} (\delta\mathbf{E} + \mathbf{v} \times \delta\mathbf{B}) \cdot \frac{\partial}{\partial \mathbf{v}} (F_\alpha + \delta f_\alpha) - C_\alpha + \langle C_\alpha \rangle_{ens} + \mathcal{D}_\alpha, \quad (3.7)$$

where

$$\begin{aligned} \frac{d}{dt} \Big|_{ens} &\equiv \frac{\partial}{\partial t} + \mathbf{v} \cdot \nabla + \frac{e_\alpha}{m_\alpha} (\mathbf{E}_0 + \mathbf{v} \times \mathbf{B}_0) \cdot \frac{\partial}{\partial \mathbf{v}}, \\ \mathcal{D}_\alpha &\equiv -\frac{e_\alpha}{m_\alpha} \left\langle (\delta\mathbf{E} + \mathbf{v} \times \delta\mathbf{B}) \cdot \frac{\partial \delta f_\alpha}{\partial \mathbf{v}} \right\rangle_{ens}. \end{aligned}$$

Now ensemble averages as well as fluctuations are expanded in powers of ρ_*

$$\begin{aligned}
 F_\alpha &= F_{\alpha 0} + F_{\alpha 1} + F_{\alpha 2} + \dots, \\
 \mathbf{E}_0 &= \mathbf{E}_{00} + \mathbf{E}_{01} + \mathbf{E}_{02} + \dots, \\
 \mathbf{B}_0 &= \mathbf{B}_{00}, \\
 \delta f_\alpha &= \delta f_{\alpha 1} + \delta f_{\alpha 2} + \dots, \\
 \delta \mathbf{E} &= \delta \mathbf{E}_1 + \delta \mathbf{E}_2 + \dots, \\
 \delta \mathbf{B} &= \delta \mathbf{B}_1 + \delta \mathbf{B}_2 + \dots.
 \end{aligned} \tag{3.8}$$

Note that we can put $\mathbf{B}_{01} = \mathbf{B}_{02} = \dots = 0$ because \mathbf{B} is used as the basis for defining the expansion parameter ρ_* [13], and also that $\mathbf{E}_{00} = -\nabla\phi_{00}$, $\mathbf{E}_{01} = -\nabla\phi_{01}$ because of the ordering $\partial\mathbf{A}/\partial t \sim \rho_*^2$. It is now possible to split Eq. 3.5 into different orders of ρ_* , and then use the gyro-phase average defined as $\langle G(\mathbf{R}, \zeta) \rangle_{\mathbf{R}} \equiv \int_0^{2\pi} d\zeta G(\mathbf{R}, \zeta) / 2\pi$ for any function $G(\mathbf{R}, \zeta)$.

Taking the gyro-phase average of the 0th order ensemble-averaged equation, $\mathcal{A}_0 = 0$, gives the lowest order equilibrium distribution

$$F_{\alpha 0} = \frac{n_\alpha(\psi, \theta)}{(2\pi T_\alpha / m_\alpha)^{3/2}} \exp\left(-\frac{m_\alpha(\mathbf{v} - \mathbf{V}_{\alpha 0})^2}{2T_\alpha}\right), \tag{3.9}$$

which is a Maxwellian in a rotating reference frame where the density can vary over a flux surface due to the centrifugal force. $\mathbf{V}_{\alpha 0}$ is the purely toroidal mean flow velocity of the species. From now on we assume that on average the plasma is not rotating toroidally and put $\mathbf{V}_{\alpha 0} = 0$. Continuing with gyro-averages of higher orders of the ensemble-averaged equation, $\mathcal{A} = 0$, results in different orders of the drift kinetic equation.

From the gyro-average of the first order perturbed equation, \mathcal{F}_1 , an expression for the first order fluctuating distribution, $\delta f_{\alpha 1}$, is obtained in terms of the distribution of the guiding centers $H_\alpha(\mathbf{R})$ as

$$\delta f_{\alpha 1}(\mathbf{r}) = -\frac{e_\alpha \delta\phi(\mathbf{r})}{T_\alpha} F_{\alpha 0} + H_\alpha(\mathbf{R}). \tag{3.10}$$

Here we can identify the first term on the right as the adiabatic response of the perturbed distribution, whereas the second term is consequently referred to as the non-adiabatic part. $H_\alpha(\mathbf{R})$ is determined by solving the nonlinear gyrokinetic equation.

It is now useful to introduce the function $h_\alpha(\mathbf{R}) = H_\alpha(\mathbf{R}) - e_\alpha F_{\alpha 0} \delta U(\mathbf{R}) / T_\alpha$ with the gyro-averaged quantity

$$\delta U(\mathbf{R}) \equiv \langle \delta\phi(\mathbf{r}) - \mathbf{v} \cdot \delta\mathbf{A}(\mathbf{r}) \rangle_{\mathbf{R}}. \tag{3.11}$$

The gyrokinetic equation is obtained from the next order perturbed equation and can, in an axisymmetric toroidal configuration with negligible toroidal rotation, be written as [12]

$$\frac{\partial h_\alpha}{\partial t} + (v_\parallel \mathbf{b} + \mathbf{v}_d) \cdot \nabla H_\alpha + \delta \mathbf{v}_d \cdot \nabla h_\alpha - C_\alpha [H_\alpha] = -\delta \mathbf{v}_d \cdot \nabla F_{\alpha 0}, \quad (3.12)$$

where \mathbf{v}_d is the drift velocity given in Eq. 2.2 with the $\mathbf{E} \times \mathbf{B}$ drift velocity subtracted [12], and we have introduced the perturbed drift velocity $\delta \mathbf{v}_d = \mathbf{b} \times \nabla \delta U / B$.

To make the equations self-consistent and couple the response of different species to each other, we use the Poisson equation and Ampère's law. We introduce the scalar electromagnetic fields $\delta A_\parallel \equiv \mathbf{b} \cdot \delta \mathbf{A}$ and $\delta B_\parallel \equiv \mathbf{b} \cdot \nabla \times \delta \mathbf{A}$ and write:

Poisson equation

$$\nabla_\perp^2 \delta \phi(\mathbf{r}) = -4\pi \sum_\alpha e_\alpha \int d^3v \delta f_\alpha(\mathbf{r}, \mathbf{v}), \quad (3.13)$$

Ampère's law

$$\begin{aligned} \nabla_\perp^2 \delta A_\parallel(\mathbf{r}) &= -4\pi \sum_\alpha e_\alpha \int d^3v v_\parallel \delta f_\alpha(\mathbf{r}, \mathbf{v}) \\ \nabla_\perp \delta B_\parallel(\mathbf{r}) \times \mathbf{b} &= 4\pi \sum_\alpha e_\alpha \int d^3v \mathbf{v}_\perp \delta f_\alpha(\mathbf{r}, \mathbf{v}). \end{aligned} \quad (3.14)$$

We approximate the perturbed distribution as $\delta f_\alpha \approx \delta f_{\alpha 1}$ from the solution to the gyrokinetic equation (Eqs. 3.10 and 3.12).

A common approach to solve space-time differential equations is to transform the problem into Fourier space. Then the equations can transform into a purely algebraic equation. However, searching for a solution to Eq. 3.12 this method leads to difficulties due to products of space-dependent quantities appearing in the equation, and Fourier transformation does not lead to an algebraic equation. Instead it is assumed that the fluctuating fields can be written as a superposition of components in the following form,

$$\delta Q(t, \mathbf{r}) = \sum_{\mathbf{k}_\perp} \delta \tilde{Q}_{\mathbf{k}_\perp}(t, \mathbf{r}) \exp(i\mathbf{k}_\perp \cdot \mathbf{r}), \quad (3.15)$$

where $\exp(i\mathbf{k}_\perp \cdot \mathbf{r})$ represents rapid variations in the direction perpendicular to the magnetic field, recalling the ordering $k_\parallel/k_\perp \sim \rho_*$. The perpendicular wave vector \mathbf{k}_\perp and $\delta \tilde{Q}_{\mathbf{k}_\perp}(t, \mathbf{r})$, as well as the ensemble-average Q_0 , are assumed to be spatially slowly varying, i.e. $\delta \tilde{Q}_{\mathbf{k}_\perp}(t, \mathbf{r}) \approx$

$\delta\tilde{Q}_{\mathbf{k}_\perp}(t, \mathbf{R})$. Using this (and recalling that $\mathbf{r} = \mathbf{R} + \boldsymbol{\rho}$) the gyro-average of one spectral component is found to be

$$\left\langle \delta\tilde{Q}_{\mathbf{k}_\perp}(t, \mathbf{R}) \exp(i\mathbf{k}_\perp \cdot \mathbf{r}) \right\rangle_{\mathbf{R}} = \delta\tilde{Q}_{\mathbf{k}_\perp}(t, \mathbf{R}) \exp(i\mathbf{k}_\perp \cdot \mathbf{R}) \langle \exp(i\mathbf{k}_\perp \cdot \boldsymbol{\rho}) \rangle_{\mathbf{R}}. \quad (3.16)$$

Gyro-averages can be evaluated in terms of the Bessel functions J_m ($m \in \mathbb{Z}$) which can be defined through

$$J_m(\varrho) = \frac{1}{2\pi} \oint d\tau \exp(-im\tau + i\varrho \sin \tau), \quad (3.17)$$

and it is possible to show that e.g.

$$\langle \exp(i\mathbf{k}_\perp \cdot \boldsymbol{\rho}) \rangle_{\mathbf{R}} = J_0(k_\perp \rho_\alpha). \quad (3.18)$$

Utilizing the gyro-averages of other terms of the form $\langle \dots \exp(i\mathbf{k}_\perp \cdot \boldsymbol{\rho}) \rangle_{\mathbf{R}}$ it is possible to rewrite $\delta U(\mathbf{R})$ (defined in Eq. 3.11) as

$$\begin{aligned} \delta U(\mathbf{R}) = J_0(k_\perp \rho_\alpha) [\delta\phi(\mathbf{R}) - v_\parallel \delta A_\parallel(\mathbf{R})] + \\ \frac{v_\perp^2}{2\Omega_\alpha} [J_0(k_\perp \rho_\alpha) + J_2(k_\perp \rho_\alpha)] \delta B_\parallel(\mathbf{R}). \end{aligned} \quad (3.19)$$

The Bessel functions represent the finite Larmor radius (FLR) effects. A possible approximation in the electrostatic case, when only J_0 appears, is to neglect them by putting $J_0(k_\perp \rho_\alpha) = 1$.

In the local approximation, each Fourier harmonics $\delta\tilde{Q}_{\mathbf{k},\omega} \exp(i\mathbf{k} \cdot \mathbf{r} - i\omega t)$ of the perturbations $\delta Q(t, \mathbf{r}) = \sum_{\mathbf{k},\omega} \delta\tilde{Q}_{\mathbf{k},\omega} \exp(i\mathbf{k} \cdot \mathbf{r} - i\omega t)$ is assumed to be independent of the other harmonics, while in reality physical inhomogeneities may couple them [11]. Nonlocal treatments take this coupling into account, hence the nonlocal eigenmode is a superposition of many coupled Fourier harmonics.

In linear gyrokinetic theory the term $\delta \mathbf{v}_d \cdot \nabla h_\alpha$, containing products of fluctuating quantities, is neglected in Eq. 3.12. This reduces the complexity substantially, but still the equations are not analytically possible to solve even in the simplest toroidal geometry. Solving them numerically is often performed only searching for the single most unstable eigenmode.

As a last remark of this section we mention that further on in this thesis perturbed quantities can also be denoted by $\hat{}$ (e.g. $\delta n_\alpha = \hat{n}_\alpha$), and the 0th order equilibrium distribution is simply denoted by $f_{\alpha 0}$ (instead of $F_{\alpha 0}$). In ballooning space the non-adiabatic part of the perturbed distribution is denoted by g and the perturbed potential by ϕ .

3.3 Ballooning formalism

Turbulent fluctuations in magnetic fusion plasmas are typically highly elongated along magnetic field lines, but have a short perpendicular scale [14, 15]. The parallel wave number k_{\parallel} and perpendicular wave number k_{\perp} follow $k_{\parallel} \sim 1/(qR) \ll k_{\perp}$ with $k_{\perp}\rho_i \sim 1$. Plasma perturbations are usually written as a superposition of components (after separating the time dependence $e^{-i\omega t}$) according to $\delta Q(r, \theta, \varphi) = \sum_{n,m} \delta \tilde{Q}_{n,m}(r) e^{i(m\theta - n\varphi)}$ [16], but in toroidal geometry the poloidal components are coupled (compare to Eq. 3.15) and the perturbation is written

$$\delta Q(r, \theta, \varphi) = \sum_{n,m} \delta \tilde{Q}_{n,m}(r, \theta) e^{i(m\theta - n\varphi)}. \quad (3.20)$$

Here we use $n, m \in \mathbb{Z}$ for the toroidal and poloidal mode numbers respectively, related to k_{φ}, k_{θ} by $k_{\varphi} = -n/R$ and $k_{\theta} = m/r$. Note that with this representation $\delta \tilde{Q}_{n,m}(r, \theta)$ has to be 2π -periodic in θ . The tokamak has unfavorable magnetic curvature on the outboard side, implying that many instabilities are more easily excited at that location. This results in a ballooning structure of the fluctuations, where the perturbations are largest in amplitude close to $\theta = 0$. Because of this ballooning-like structure, it is not efficient to represent perturbations according to Eq. 3.20. We are interested in a set of mode numbers such that $m = nq$, but then the representation of δQ in Eq. 3.20 is only useful on a flux surface where q is a rational number since the perturbation should be 2π -periodic in θ and φ . For non-zero magnetic shear q is irrational at an infinitesimal distance away from a rational surface.

Because of the elongated linear mode structure nq is large, which implies that the rational surfaces are close to each other. Hence the microinstabilities radially extend over several rational surfaces rather than being localized around one. It is thus more convenient to write the perturbation in the ballooning representation [14, 17], appropriate for describing mode structures characterized by long parallel wavelength and short perpendicular wavelength when the magnetic shear is finite. The n^{th} toroidal harmonic of the perturbation can be expressed as $\delta Q_n(r, \theta, \varphi) = \delta \tilde{Q}_{n,m}(r, \theta) e^{-in[\varphi - q(r)\theta]}$. We rewrite this harmonic in terms of an extended poloidal angle $\vartheta = \theta + 2\pi j \in \mathbb{R}$ ($j \in \mathbb{Z}$) as

$$\delta Q_n(r, \theta, \varphi) = \sum_{\theta_0} \sum_{j=-\infty}^{\infty} \delta \tilde{Q}_{B,n}(\vartheta, \theta_0) e^{-in[\varphi - q(r)(\vartheta + \theta_0)]}, \quad (3.21)$$

where also the ballooning angle θ_0 has been introduced. ϑ is basically a coordinate along the field line, while θ_0 is the real poloidal angle where the wave fronts are perpendicular to the flux surface. $\tilde{Q}_{B,n}(\vartheta, \theta_0)$ does not have a periodicity condition, only the requirement that $\tilde{Q}_{B,n}(\vartheta, \theta_0) \rightarrow 0$ as $|\vartheta| \rightarrow \infty$. To calculate the most unstable mode it is usually enough to consider the $\theta_0 = 0$ term, so for practical purpose we can make the approximation

$$\delta Q_n(r, \theta, \varphi) \approx \sum_{j=-\infty}^{\infty} \delta \tilde{Q}_{B,n}(\vartheta) e^{-in[\varphi - q(r)\vartheta]}, \quad (3.22)$$

where $\delta \tilde{Q}_{B,n}(\vartheta) \equiv \delta \tilde{Q}_{B,n}(\vartheta, 0)$.

In ballooning representation the eigenmodes are radially periodic, which means that it is only a realistic representation if the plasma parameters are constant over the considered radial domain. Making this approximation can be justified in the $\rho_* \rightarrow 0$ limit, i.e. when the plasma size is much larger than the radial domain. This is called flattening of the profiles, and is often used in simulations to relax the computational task.

3.3.1 Gyrokinetic equation in ballooning space

The linearized gyrokinetic equation for the non-adiabatic part of the perturbed distribution g_α is in ballooning space given by (i.e. $g = g_{B,n}(\vartheta)$) [18]

$$\left. \frac{v_{\parallel}}{qR} \frac{\partial g_\alpha}{\partial \vartheta} \right|_{\mathcal{E}, \mu} - i(\omega - \omega_{D\alpha} - \omega_E)g_\alpha - C[g_\alpha] = -i \frac{e_\alpha f_{\alpha 0}}{T_\alpha} (\omega - \omega_{*\alpha}^T) \phi J_0(z_\alpha), \quad (3.23)$$

for a low- β , circular cross section, axisymmetric, large aspect ratio equilibrium and in the presence of a poloidally varying equilibrium potential ϕ_E , where only pure electrostatic perturbations are considered ($\phi(\vartheta)$ is the perturbed potential in ballooning space) and we neglect plasma rotation. Note that the time derivative is expressed in terms of wave frequency, i.e. $\partial/\partial t \rightarrow -i\omega$. Here $f_{\alpha 0} = n_{\alpha 0}(m_\alpha/2\pi T_\alpha)^{3/2} \exp(-\mathcal{E}/T_\alpha)$ is an equilibrium Maxwellian distribution function, $n_\alpha(\mathbf{r}) = n_{\alpha 0} \exp[e_\alpha \phi_E(\mathbf{r})/T_\alpha]$ is the poloidally varying density and $n_{\alpha 0}$ is a flux function. The diamagnetic frequency is defined as $\omega_{*\alpha} = -k_\theta T_\alpha / e_\alpha B L_{n\alpha}$ and $\omega_{*\alpha}^T = \omega_{*\alpha} [1 + (x^2 - 3/2) L_{n\alpha} / L_{T\alpha}]$, where $x = v/v_{T\alpha}$ represents velocity normalized to the thermal speed $v_{T\alpha} = (2T_\alpha/m_\alpha)^{1/2}$. The

magnetic drift frequency is $\omega_{D\alpha} = -2k_\theta T_\alpha (x_\perp^2/2 + x_\parallel^2) \mathcal{D}(\vartheta) / (m_\alpha \Omega_\alpha R)$, with $\mathcal{D}(\vartheta) = \cos \vartheta + s\vartheta \sin \vartheta$. The argument to the Bessel function is $z_\alpha = k_\perp v_\perp / \Omega_\alpha$, with $k_\perp = (1 + s^2 \vartheta^2)^{1/2} k_\theta$, and it is responsible for the FLR effects. The $\mathbf{E} \times \mathbf{B}$ drift frequency of the particles in the equilibrium electrostatic field is $\omega_E = -\frac{k_\theta}{B} \frac{s\vartheta}{r} \frac{\partial \phi_E}{\partial \vartheta}$, and was derived in Appendix A of paper A. Note that usually this term is left out of the equation, because it only exists if there is a local poloidal (or radial) variation in the equilibrium potential which can often be neglected. However under certain conditions, and in particular when describing high- Z impurities, its magnitude can be comparable to the other terms and thus have to be included. The leftmost term of Eq. 3.23, $v_\parallel / (qR) \partial g_\alpha / \partial \vartheta$, is referred to as the parallel compressibility (or parallel dynamics). Sometimes this term does not affect the linear mode structure significantly, and it is therefore common in simulation packages to allow for the possibility to neglect it. This can e.g. be used when studying the toroidal ITG mode mentioned in Sec. 3.1.1, but it can also be advantageously used to study the impact of the term itself. Although ignoring parallel compressibility can lead to reasonable estimates for linear growth rates, this simplification does not give the correct nonlinear evolution of modes [11], and should thus only be considered for linear simulations. Most of the work in this thesis is based on Eq. 3.23, and we will return to it further on.

3.4 Turbulent fluxes

The overriding goal of transport theory in magnetic fusion plasmas is to determine the cross-field fluxes of e.g. particles and energy. These fluxes can be theoretically divided into collisional and anomalous components, e.g. $\Gamma = \Gamma_{\text{CO}} + \Gamma_{\text{AN}}$, where the anomalous component often dominates over the collisional. The anomalous component represents the ensemble-average of the flux due to turbulent fluctuations [10].

Focusing on electrostatic turbulence, a potential perturbation $\delta\phi$ gives rise to a perturbed drift velocity $\delta\mathbf{v}_d = \mathbf{b} \times \nabla \delta U / B$ with $\delta U = \delta\phi$ from Eq. 3.11. This produces a particle flow, which can be averaged over a flux surface to obtain the cross-field particle flux through the surface $\Gamma_{\alpha\perp}$ as [13, 16]

$$\Gamma_{\alpha\perp} = \langle \text{Re} [\delta n_\alpha \delta \mathbf{v}_d^* \cdot \hat{r}] \rangle, \quad (3.24)$$

where $\text{Re}[\dots]$ denotes the real part, $*$ the complex conjugate and \hat{r} is the radial unit vector. The perturbed density is obtained by taking the

0th moment of the perturbed distribution function, consequently it can be seen from Eq. 3.23 (recall that ϕ in Eq. 3.23 corresponds to $\delta\phi$ here) that $\delta n_\alpha \propto \delta\phi$. This can also be verified from Eq. 3.12 in the nonlinear case. This proportionality is also true for the temperature perturbation since it is a higher order moment of the same perturbed distribution. We now note that we can use $\delta\mathbf{v}_d^* \cdot \hat{\mathbf{r}} = \mathbf{b} \times \nabla\delta\phi^*/B \cdot \hat{\mathbf{r}} = ik_\theta\delta\phi^*/B$ to rewrite Eq. 3.24 and obtain the particle flux as

$$\Gamma_{\alpha\perp} = - \left\langle \frac{k_\theta}{B} \text{Im} [\delta n_\alpha \delta\phi^*] \right\rangle, \quad (3.25)$$

where $\text{Im}[\dots]$ denotes the imaginary part. Similarly the energy flux is found to be

$$Q_{\alpha\perp} = - \left\langle \frac{k_\theta}{B} n_\alpha \text{Im} [\delta T_\alpha \delta\phi^*] \right\rangle. \quad (3.26)$$

From Eq. 3.24 we make the important observation, that if the “transporter” $\delta\mathbf{v}_d$ and the “transportee” δn_α are 90° out of phase there is no net transport of particles. Equivalently Eqs. 3.25 and 3.26 reveal that turbulent particle (energy) fluxes only occur when the perturbed density (temperature) and the perturbed potential are out of phase. This leads to the immediate conclusion that the adiabatic response, described by Eq. 3.1, does not contribute to the cross-field particle fluxes.

As mentioned earlier, linear gyrokinetic theory is implemented by neglecting all terms in the gyrokinetic equation containing products of fluctuating quantities. The anomalous fluxes obtained in this theory are referred to as the *quasilinear* fluxes [10]. In linear theory only the most unstable mode is usually analyzed (although it is possible to search for sub-dominant modes). If an instability exists, the linear growth rate $\gamma > 0$ and the perturbed quantities $\delta Q \propto \exp(i\mathbf{k} \cdot \mathbf{r} - i\omega_r t + \gamma t)$ grow exponentially in time indefinitely. We realize that such a behavior is unphysical. As the fluctuating amplitudes increase, saturation from nonlinear mode-coupling becomes more and more important, and the quasilinear approximation breaks down. A consequence of this is that it is not possible calculate the absolute anomalous fluxes from a quasilinear approach, to do that one has to resort to nonlinear transport theory. To estimate the fluxes in quasilinear transport theory a common approach is to estimate the magnitude of the perturbed potential based on a so-called *mixing length* approximation. This procedure is a crude way of associating an instability with a random walk picture [10].

As a final remark of this section, we note that in a local flux-tube limit (described in Sec. 3.6) one can prove, by summing the averaged par-

ticle fluxes over species and using Maxwell's equations, that the anomalous fluxes possess the ambipolarity property [12, 13]

$$\sum_{\alpha} e_{\alpha} \Gamma_{\alpha\perp} = 0. \quad (3.27)$$

Ambipolarity implies that on average the electric current is zero in the cross-field direction.

3.5 Collisions

In the absence of microinstabilities the cross-field particle and energy transport is completely determined by collisional processes, but naturally collisions play an important role in turbulent transport as well. Due to the long range nature of the Coulomb interaction, and that the number of particles within a Debye sphere of a plasma is large, each particle is constantly in interaction with a large number of other particles. Small angle-scattering dominates over large deflections, and a single particle follows a smooth trajectory. The collision operator $C_{\alpha}[f_{\alpha}] = \sum_b C_{ab}[f_{\alpha}, f_b]$ describes the change in distribution f_{α} of species α due to interaction with all plasma species b , and is truly complicated to treat. A realistic collision operator should conserve particles, momentum and energy, and in its most sophisticated form C_{ab} is given by the Fokker-Planck collision operator (see e.g. Eq. (3.21) of Ref. [7]). In practice due to its complexity this form is often intractable to use, even with the best simulation tools available, and one has to resort to simplifications. Approximations can be made in special cases such as when the colliding species have significantly different masses, or for a species colliding with a Maxwellian background, but these approximations can also be difficult to implement. One crucial property of a useful collision operator is that it should drive the system towards local thermodynamic equilibrium. Importantly for two Maxwellian distributions $f_{M\alpha}, f_{Mb}$ with equal temperatures and mean velocities, the relative collision operator should vanish, $C_{ab}[f_{M\alpha}, f_{Mb}] = C_{b\alpha}[f_{Mb}, f_{M\alpha}] = 0$.

Due to the smoothness of Coulomb collisions, it is common to define the collision time τ as the time required for an order unity relative change in velocity of a particle as a result of the cumulative interaction with other particles. The collision frequency is then defined as $\nu = \tau^{-1}$.

The electron-ion collision frequency can be shown to be [7]

$$\nu_{ei} \propto \frac{e^4 n_i Z_i^2 \ln \Lambda}{\epsilon_0^2 m_e^{1/2} T_e^{3/2}}, \quad (3.28)$$

where ϵ_0 is the electric permittivity of free space and $\ln \Lambda$ the Coulomb logarithm. Furthermore, assuming $T_i = T_e$, it can be shown that $\nu_{ei} = \nu_{ii} \sqrt{m_i/m_e} / Z_i^2 = \nu_{ie} m_i / m_e$ and $\nu_{ee} \sim \nu_{ei}$. Since the collision frequency is inversely proportional to $T^{3/2}$, it can be justified to neglect collisions in hot parts of fusion plasmas such as close to the core. However, both simulations and experiments have shown that collisions can affect turbulent transport significantly [19] and often a model of collisions should be included for completeness. A highly simplified model, with the advantage that it is easy to treat, is the Krook operator $C_\alpha[f_\alpha] = -\nu(f_\alpha - f_{M\alpha})$ which simply drives the distribution towards a Maxwellian $f_{M\alpha}$. Here the collision frequency ν can include an energy dependence.

A more advanced collision operator is the pitch-angle scattering operator (or Lorentz operator)

$$\mathcal{L}[f_\alpha] \equiv \frac{1}{2} \frac{\partial}{\partial \xi} \left[(1 - \xi^2) \frac{\partial f_\alpha}{\partial \xi} \right], \quad (3.29)$$

where $\xi = v_{\parallel}/v$ is the cosine of the pitch-angle. This operator describes diffusion on a surface of constant velocity, thus changing the direction but not the magnitude of the velocity vector. As an example it is useful for describing electrons colliding with the much heavier ions, $C_{ei}[f_e, f_i] \approx \nu_{ei}(v) \mathcal{L}[f_e]$, but can be the dominant contribution in other cases as well.

Lastly, for a system close to local thermodynamic equilibrium (when the distribution is nearly Maxwellian, $f_\alpha = f_{M\alpha} + f_{\alpha 1}$ with $f_{\alpha 1} \ll f_{M\alpha}$) the linearized collision operator $C_{\alpha\alpha}^{(l)}[f_\alpha] \equiv C_{\alpha\alpha}[f_{\alpha 1}, f_{M\alpha}] + C_{\alpha\alpha}[f_{M\alpha}, f_{\alpha 1}]$ can be useful for describing collisions between particles of the same species. Besides being linear, and conserving particles, momentum and energy, it has the important property of being self-adjoint which means that any two functions $\hat{f}(\mathbf{v})$, $\hat{g}(\mathbf{v})$ satisfy $\int \hat{g} C_{\alpha\alpha}^{(l)}[f_{M\alpha} \hat{f}] d^3v = \int \hat{f} C_{\alpha\alpha}^{(l)}[f_{M\alpha} \hat{g}] d^3v$.

3.6 Gyrokinetic simulations

Today several different packages exist to simulate radial anomalous transport from microturbulence in tokamaks using the gyrokinetic approach, both particle-in-cell codes as well as codes using grids are available. In the local approximation they commonly work by specifying plasma parameters such as the geometry and local gradients, furthermore the temporal and spatial domain and resolution of the simulation, number of eigenmodes and mode numbers, etcetera. The computed output is the perturbed quantities, mode frequencies and turbulent fluxes. The simulation domain is typically a flux tube following the magnetic field lines, with a radial and binormal extent. The domain size in all three spatial dimensions has to be significantly larger than the correlation length of the turbulence. For this type of domain it is convenient to use a field aligned coordinate system. The plasma parameters and gradients can be approximated as constants over the perpendicular simulation domain in the limit $\rho_* \rightarrow 0$. Local flux-tube simulations normally use periodic radial boundary conditions, while global simulations allow for non-periodic boundary conditions and can be useful for analyzing e.g. non-local effects.

Linear gyrokinetic simulations typically only search for one toroidal eigenmode, which grows exponentially and never saturates due to the absence of nonlinear mode-coupling. This implies that it is not possible to calculate the magnitude of the perturbed quantities, and thus neither the absolute fluxes, in contrast to nonlinear simulations. However it is still possible to determine if the analyzed mode contribute to inward or outward radial transport linearly, i.e. in the absence of mode-coupling. Linear simulations usually use an initial value technique to find the most unstable mode, but it can also be possible to search for sub-dominant modes using eigenvalue solvers.

Nonlinear simulations are run until the system reaches a state of fully developed turbulence, when the fluctuating quantities have reached an amplitude where nonlinear mode coupling becomes important. This state is statistically independent of the initial conditions. After reaching the turbulent state, the simulation has to continue running long enough for the statistical properties of the output quantities to be correctly determined.

Gyrokinetic simulation of turbulent transport is a heavy numerical task, specially nonlinear simulations typically require vast computer resources for the statistics to be good enough. Today's rapid development

of supercomputers have enabled a more extensive utilization of gyrokinetic simulations, but still it is a tedious task to produce larger amounts of nonlinear results. Linear simulations are significantly less expensive, and can in several situations be used for qualitative predictions. To calculate turbulent fluxes it can be useful to resort to fluid simulations which, despite not being as accurate, normally are much faster than nonlinear gyrokinetic simulations.

In the present thesis results are obtained from simulations with GYRO [20, 21]. GYRO, developed at General Atomics, USA, is a nonlinear tokamak microturbulence package using a fixed Eulerian grid to solve the 5D gyrokinetic-Maxwell equations. It is able to treat a local flux-tube domain or a global radial domain in a full or partial torus with a general shaped plasma cross section.

3.7 Impurity transport

Impurities are ubiquitous in fusion plasmas. They enter in form of alpha particles (${}^4\text{He}^{2+}$) as a rest product of the D-T fusion reaction, but also from plasma interaction with the surrounding wall. In the core of a fusion plasma the fusion reactivity should be high. Since impurities lead to plasma dilution and radiative energy losses, impurity accumulation in the core must be avoided. As mentioned earlier high- Z impurities are particularly detrimental. In recent years it has been observed experimentally that plasma heating by RF waves close to the center can result in a reduction of the impurity content in the core (see Fig. 3.1) [22]. An effect which lacks a complete theoretical understanding, but could possibly be connected to a poloidal redistribution of the impurity species over a flux surface. This redistribution has been observed experimentally in tokamaks (see Fig. 3.1) [23]. Reference [24] includes an explanation of how an impurity species can become poloidally asymmetrically distributed under ICRH of a minority species, and [25] presents a theoretical model for the link between the asymmetry strength and the ICRH.

This thesis addresses the topic of turbulent cross-field transport of high- Z impurities present in trace quantities $Zn_z/n_e \ll 1$, including the situation when a poloidally varying equilibrium potential ϕ_E is present. The trace limit is experimentally relevant, and implies that the turbulent modes driving the transport are unaffected by the presence of the impurities. When larger quantities of impurities are present how-

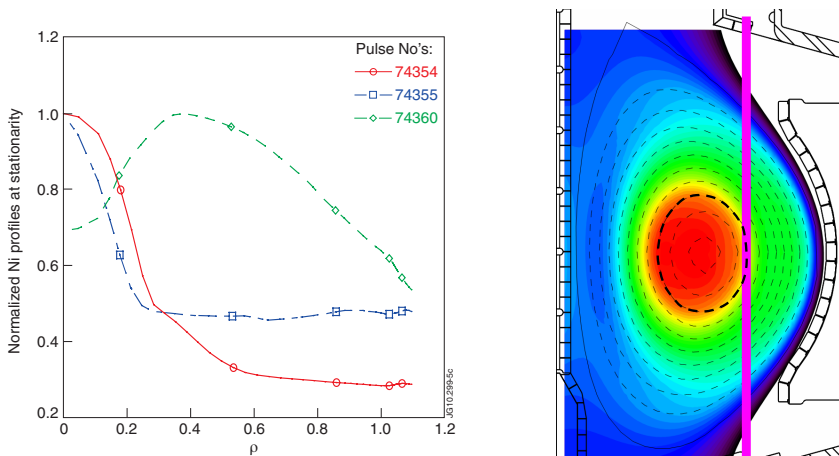


Figure 3.1: The left figure shows the normalized nickel density profiles (here ρ is the radial coordinate) for three discharges in the JET tokamak with no heating power (74354), 1 MW (74355) and 3 MW (74360) of ICRH, respectively (figure from [22]). The right figure illustrates how applying ICRH with the resonance location at the low-field-side (highlighted with pink line), can lead to a poloidally asymmetrically distributed impurity species in the ALCATOR C-Mod tokamak (courtesy of M. L. Reinke).

ever it will affect the structure of the turbulence. A model for ϕ_E is introduced as Eq. 11 of Paper A. This model implies that the impact of the poloidal variation is mainly on high- Z impurities due to their high charge, while the main species remain almost unaffected. As a consequence we can obtain the eigenvalues ω and the perturbed potential ϕ of the most unstable mode from linear gyrokinetic simulations with GYRO, neglecting the varying equilibrium potential. The solution is substituted into Eq. 3.23 to give g_z . To analyze the turbulent radial impurity transport we calculate the zero-flux impurity density gradient (the peaking factor) obtained by requiring that the flux surface averaged linear impurity flux Γ_z should vanish, $0 = \langle \Gamma_z \rangle \equiv - \left\langle \text{Im} \left[\frac{k_\theta}{B} \hat{n}_z \phi^* \right] \right\rangle = - \left\langle \text{Im} \left[\frac{k_\theta}{B} \int d^3 v J_0(z_z) g_z \phi^* \right] \right\rangle$, here \hat{n}_z is the perturbed impurity density. In other words, the peaking factor a/L_{nz}^0 represents the (normalized) impurity density gradient in a steady state far from impurity sources, where a negative value implies that the impurity density increases in radial direction (see Fig. 3.2). Consequently it is interesting to look for scenarios where the peaking factor is negative close to the plasma core.

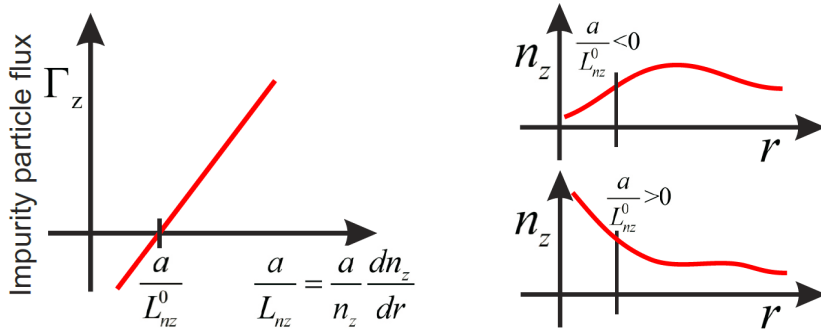


Figure 3.2: The left figure illustrates the definition of the impurity peaking factor a/L_{nz}^0 as the value of a/L_{nz} when $\langle \Gamma_z \rangle = 0$. The right figure shows how the local impurity density varies when $a/L_{nz}^0 < 0$ and $a/L_{nz}^0 > 0$ respectively. If $a/L_{nz}^0 \geq 0$ everywhere inside the tokamak plasma, the impurity density profile is peaked. Otherwise it is hollow.

Chapter 4

Summary

The present thesis treats aspects of turbulent radial transport of high- Z impurities in tokamaks. In particular we study how the presence of poloidal asymmetries affect the radial impurity transport. The main part is devoted to quasilinear studies of electrostatic turbulence, but also a study of electromagnetic drift waves is included.

In paper [A](#) electrostatic impurity transport close to the core in the presence of a poloidally varying equilibrium potential ϕ_E is studied, which introduces a non-negligible modification to the particle orbits in the GK equation (Eq. [3.23](#)) for high- Z impurities. A simple sinusoidal model for ϕ_E is suggested as $Ze\phi_E/T_z = -\kappa \cos(\theta - \delta)$, based on the effect of minority ion redistribution over a flux surface when applying ICRH on the low field side. Here κ is the asymmetry strength, depending on e.g. heating power and resonance location, while δ is the angular position of the impurity maximum ($\delta = \pi$ in the case of low field side ICRH). We assume that $e\phi_E/T_\alpha \ll 1$ implying that the main species are almost unaffected by the varying potential, while $Ze\phi_E/T_z \sim \mathcal{O}(1)$ so that the impurities are affected due to their high charge. The eigenvalues and perturbed potential of the most unstable mode are therefore obtained by linear gyrokinetic flux-tube simulations with GYRO in the poloidally symmetric case, assuming large-aspect ratio and circular cross section. We find that our baseline case is dominated by ITG turbulence. The results indicate that the conclusions are general for any high- Z impurity species present in trace quantities. It should be noted that in this particular work the parallel dynamics of main ions and impurities is neglected to simplify the analytical treatment, this implies that $v_{\parallel}/(qR) \partial g_\alpha / \partial \vartheta = 0$ in Eq. [3.23](#). Furthermore also FLR effects for the

impurities are omitted by putting $J_0(z_z) = 1$. Collisions are modeled by a Lorentz operator. The solution from GYRO is substituted into Eq. 3.23 for impurities, which is then solved using a variational approach having the non-adiabatic distribution given by a truncated Legendre polynomial series in the pitch angle parameter $\xi = x_{\parallel}/x$.

The results suggest that the poloidal asymmetry strength and magnetic shear are the two most important parameters that affect the impurity peaking. Furthermore a strong enough asymmetry can even lead to a negative impurity density gradient in steady state, which would imply that impurities do not accumulate in the core of the tokamak.

Paper B extends the work of Paper A analyzing the same baseline case but keeping the ion/impurity parallel dynamics, the FLR effects and using the more sophisticated linearized impurity-impurity collision operator $C_{zz}^{(l)}$ (the ordering $n_z Z^2/n_e \sim \mathcal{O}(1)$ implies that impurity self-collisions dominate over collisions with unlike species). A perturbative solution to Eq. 3.23 in the small parameter $Z^{-1/2}$ is constructed, keeping terms up to $\mathcal{O}(Z^{-1})$. The subsequent semi-analytical expression (Eq. (8) in paper B) for the impurity peaking factor interestingly shows that up to order Z^{-1} the peaking is independent of both FLR effects and collisionality. This expression essentially shows that the impurity peaking is determined by three separate contributions: one coming from the magnetic drifts, another from the $\mathbf{E} \times \mathbf{B}$ drift in the poloidally varying equilibrium potential, and a third arising due to the parallel impurity dynamics. It is seen that this last contribution typically leads to an increased impurity peaking for ITG turbulence, while the opposite could be expected for TE turbulence.

In paper C the analysis is focused on collisionless TE modes driven by the density gradients or the electron temperature gradient, and includes a thorough investigation of their impact on impurity transport. The main part of the work is devoted to quasilinear studies and the same approximate solution for the impurity peaking factor is used as in paper B. However to estimate the validity of the linear results we include some results from nonlinear GYRO simulations and it is found that they conform quite well. Although the poloidally varying equilibrium potential (and the arising $\mathbf{E} \times \mathbf{B}$ drift) is still included in the analysis, much of the attention of the paper is focused on the contribution to the impurity peaking related to the parallel impurity dynamics. For TE modes this contribution typically decreases the peaking factor, which is verified by quasilinear GYRO simulations. It is shown that the mode characteristics,

and particularly the factor $\omega_r / (\omega_r^2 + \gamma^2)$, together with the safety factor are important for determining the magnitude of the parallel dynamics contribution. Furthermore for TE modes driven by the electron temperature gradient the peaking factor is found to be close to 0 or negative, even in the poloidally symmetric case.

In the last part of the thesis, paper D, the attention is drawn towards quasilinear impurity transport driven by electromagnetic turbulence, relevant in scenarios where β is high enough. Besides ITG modes also kinetic ballooning modes (KBM) are analyzed which only appear at finite β . Increasing β from 0 reduces the linear growth rate of an ITG mode until a critical value is reached where a KBM becomes the most unstable mode. For KBM modes the growth rate dependence on β is found to be non-monotonic. The results show that the value of β can affect the impurity peaking, and that the impurity peaking factor is typically lower in KBM turbulence than in ITG turbulence. Furthermore we find that the charge-to-mass ratio of the impurity species affect the peaking factor in ITG turbulence, by changing the magnitude of the contribution related to parallel dynamics (this is expected from Eq. (8) of paper B).

In summary this thesis analyzes the density peaking of high- Z impurities present in trace quantities in tokamak plasmas. The role of electromagnetic effects is investigated and we show that they can significantly affect the turbulent cross-field impurity transport. In the electrostatic case, a semi-analytical model for the impurity peaking is introduced, which includes the effect of a poloidally varying equilibrium potential. Such a potential could arise e.g. when applying ICRH to a minority ion species on the low field side, and will then cause high- Z impurities to accumulate on the inboard side. We demonstrate that the varying potential can affect the cross-field impurity transport considerably, and reduce the impurity peaking. Besides the asymmetry strength, magnetic shear is a key parameter in determining the size of this effect. Furthermore we analyze how the contribution from parallel dynamics affect the impurity peaking. We find that its magnitude is mainly governed by the mode characteristics and the safety factor.

References

- [1] Chen, F.F. *An Indispensable Truth: How Fusion Power Can Save the Planet*. Springer (2011). ISBN 978-1-4419-7819-6. <http://dx.doi.org/10.1007/978-1-4419-7820-2>.
- [2] McCracken, G. and Stott, P. *Fusion: The energy of the Universe*. Elsevier Academic Press (2005). ISBN 0-12-481851-X.
- [3] Freidberg, J. *Plasma Physics and Fusion Energy*. Cambridge University Press (2007). ISBN 978-0-521-73317-5.
- [4] *All-the-World's Tokamaks*. www.tokamak.info.
- [5] Romanelli, F. et al. *Fusion Electricity - EFDA*. Garching, Germany (2012). ISBN 978-3-00-040720-8. <http://www.efda.org/newsletter/the-road-to-fusion-electricity/>.
- [6] *ITER webpage*. <http://www.iter.org/>.
- [7] Helander, P. and Sigmar, D.J. *Collisional transport of magnetized plasmas*. Cambridge University Press, Cambridge (2002). ISBN 978-0-521-80798-2.
- [8] Wesson, J. *Tokamaks*. Clarendon Press, Oxford, third edition (2004). ISBN 978-0-19-850922-6. <http://www.iop.org/EJ/abstract/0741-3335/46/3/173515>.
- [9] Kikuchi, M., Lackner, K. and Tran, M.Q. *Fusion physics*. International Atomic Energy Agency (2012). ISBN 978-92-0-130410-0. <http://www-pub.iaea.org/books/IAEABooks/8879/Fusion-Physics>.
- [10] Balescu, R. *Aspects of Anomalous Transport in Plasmas*. Institute of Physics Publishing (2005). ISBN 9780750310307.

- [11] Beer, M.A. Gyrofluid models of turbulent transport in tokamaks. Ph.D. thesis, Princeton University (1995).
- [12] Candy, J. and Belli, E. GYRO technical guide. Technical report, General Atomics, San Diego, CA, USA (2012). <https://fusion.gat.com/theory/Gyrodoc>.
- [13] Sugama, H. and Horton, W. Nonlinear electromagnetic gyrokinetic equation for plasmas with large mean flows. *Phys. Plasmas*, **5** (1998), 2560. http://pop.aip.org/resource/1/phpaen/v5/i7/p2560_s1.
- [14] Connor, J.W., Hastie, R.J. and Taylor, J.B. Stability of general plasma equilibria. *Plasma Physics*, **22** (1980), 757–769. <http://iopscience.iop.org/0032-1028/22/7/013>.
- [15] Pusztai, I. Turbulent and neoclassical transport in tokamak plasmas. Ph.D. thesis, Chalmers University of Technology (2011). http://ft.nephy.chalmers.se/publications/pusztai_phd_thesis.pdf.
- [16] Weiland, J. *Collective Modes in Inhomogeneous Plasma*. Institute of Physics Publishing (2000). ISBN 0750305894.
- [17] Connor, J.W., Hastie, R.J. and Taylor, J.B. Shear, Periodicity, and Plasma Ballooning Modes. *Phys. Rev. Lett.*, **40** (1978), 396–399. http://prl.aps.org/abstract/PRL/v40/i6/p396_1.
- [18] Romanelli, F. and Briguglio, S. Toroidal semicollisional microinstabilities and anomalous electron and ion transport. *Phys. Fluids B*, **2** (1990), 754. http://pop.aip.org/resource/1/pfbpei/v2/i4/p754_s1.
- [19] Angioni, C. et al. Density Peaking, Anomalous Pinch, and Collisionality in Tokamak Plasmas. *Phys. Rev. Lett.*, **90** (2003), 205003. <http://prl.aps.org/abstract/PRL/v90/i20/e205003>.
- [20] Candy, J. and Waltz, R.E. An Eulerian gyrokinetic-Maxwell solver. *J. Comput. Phys.*, **186** (2003), 545–581. <http://www.sciencedirect.com/science/article/pii/S0021999103000792>.
- [21] *GYRO webpage*. <https://fusion.gat.com/theory/Gyro>.

-
- [22] Valisa, M. et al. Metal impurity transport control in JET H-mode plasmas with central ion cyclotron radiofrequency power injection. *Nucl. Fusion*, **51** (2011), 033002. <http://iopscience.iop.org/0029-5515/51/3/033002/cites>.
- [23] Reinke, M.L. et al. Poloidal variation of high-Z impurity density due to hydrogen minority ion cyclotron resonance heating on Alcator C-mod. *Plasma Phys. Control. Fusion*, **54** (2012), 045004. <http://iopscience.iop.org/0741-3335/54/4/045004/>.
- [24] Ingesson, L.C. et al. Comparison of basis functions in soft x-ray tomography and observation of poloidal asymmetries in impurity density. *Plasma Phys. Control. Fusion*, **42** (2000), 161–180. <http://iopscience.iop.org/0741-3335/42/2/308>.
- [25] Kazakov, Y.O. et al. Poloidal asymmetries due to ion cyclotron resonance heating. *Plasma Phys. Control. Fusion*, **54** (2012), 105010. <http://iopscience.iop.org/0741-3335/54/10/105010/>.

REFERENCES
